Meridional Migration of Tropical Convergence Zones

J. SRINIVASAN

Center for Atmospheric Sciences, Indian Institute of Science, Bangalore, India

G. L. SMITH

Atmospheric Sciences Division, NASA/Langley Research Center, Hampton, Virginia

(Manuscript received 5 June 1995, in final form 7 December 1995)

ABSTRACT

Outgoing longwave radiation data from the Earth Radiation Budget Experiment show that the meridional migration of tropical convergence zones (TCZ) varies greatly from one region to another in the Tropics. In Africa, the meridional migration of TCZ is limited due to the meridional variation of the planetary net radiation due to the Sahara Desert. The large meridional migration in the Asian subcontinent and the west Pacific Ocean is attributed to the strong land–sea contrast in these regions. The wind–evaporation feedback mechanism is proposed as the cause of intraseasonal meridional migration of TCZ in the Atlantic and east Pacific Oceans.

1. Introduction

The intraseasonal variation of the climate in the Tropics is influenced strongly by the zonal and meridional migration of convergence zones. The zonal migration of tropical convergence zones (TCZ) has been studied extensively because it is associated with the 30–50-day Madden–Julian oscillation (see review by Madden and Julian 1994). The meridional migration of TCZ has not received as much attention because substantial meridional migration of TCZ is observed in the Indian and west Pacific Oceans only. This paper presents an investigation of the intraseasonal meridional migration of TCZ in various regions of the Tropics using outgoing longwave radiation (OLR) from the Earth Radiation Budget Experiment (ERBE).

The OLR data are examined by latitude–time sections and show a wide variety of behaviors in different regions around the equator and throughout the year of data that is examined. The characteristics of the meridional migrations of the TCZ and the governing mechanisms are discussed for the different regions. It is assumed that 1986 is a "representative" year for this purpose, although in the Tropics the El Niño/Southern Oscillation (ENSO) can have a major effect. In this regard we note that during 1986 the ENSO was in a cool phase. Meridional migrations of the TCZ take place on various timescales ranging from the annual movement to more rapid waves, with a timescale of several days. In many case, the observations support and are explained by theoretical studies of several investigators.

Sikka and Gadgil (1980) identified the existence of northward migration of TCZ in the longitude region 70°–90°E by using visible satellite imagery. Gadgil and Srinivasan (1990) used a bispectral threshold technique (i.e., both OLR and albedo) with data from the National Oceanic and Atmospheric Administration Advanced Very High Resolution Radiometer (AVHRR) to identify TCZ and displayed the pattern of meridional propagation in different regions of the Tropics. They employed an albedo threshold to remove the cirrus clouds and spatial filtering to retain the largest scales. The use of an albedo threshold method introduced a bias because daytime data alone can be used. Recent studies (see, for example, Minnis and Harrison 1984) indicated the presence of strong diurnal variation of OLR in both oceanic and continental regions. The ERBE data are processed to account for the diurnal cycle (Barkstrom and Smith 1986; Brooks et al. 1986). Thus, ERBE OLR data were selected for the present study in order to minimize the effects of the diurnal cycle on the observations of the TCZ movements.

Wang and Rui (1990) used a pentad mean outgoing longwave radiation (OLR) anomaly to study the climatology of zonally and meridionally propagating TCZ that they called tropical intraseasonal convection anomaly (TICA). Wang and Rui (1990) presented pentad mean OLR anomaly maps by averaging over 15° lati-

Corresponding author address: Dr. G. Louis Smith, Atmospheric Sciences Division, NASA/Langley Research Center, Mail Code 420, Hampton, VA 23681-0001.

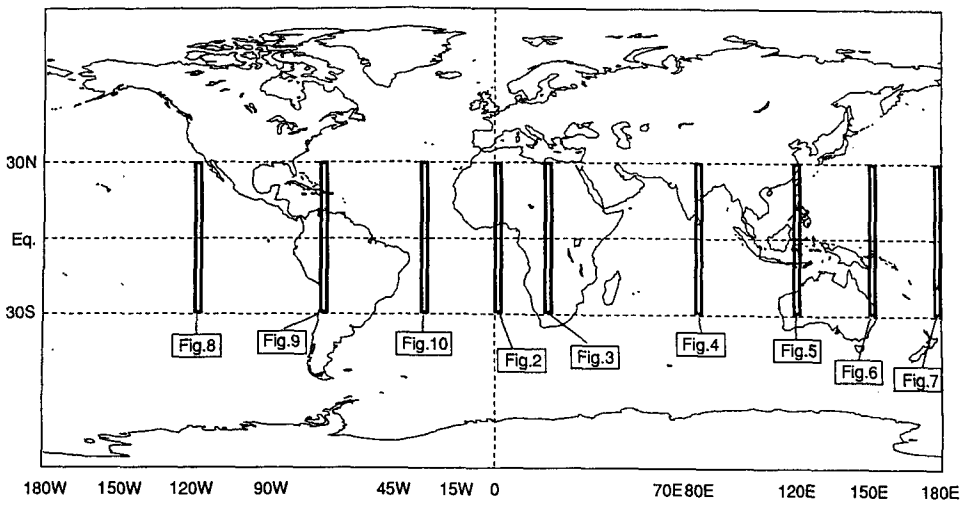

FIG. 1. Map of earth showing 2.5° regions that were used to create the latitude–time images in Figs. 2–10.

tude and 35° longitude. The large spatial filtering in the meridional direction can obscure the nature of meridional migration because the meridional excursion of TCZ is usually less than 20° in latitude. Seager and Zebiak (1994) argued that spatial and temporal filtering can obscure the real nature of the intraseasonal oscillation and its relation to the stationary features of the circulation and the seasonal cycle. We believe that the rich structure of tropical intraseasonal oscillation is more evident if the daily OLR data are used with no

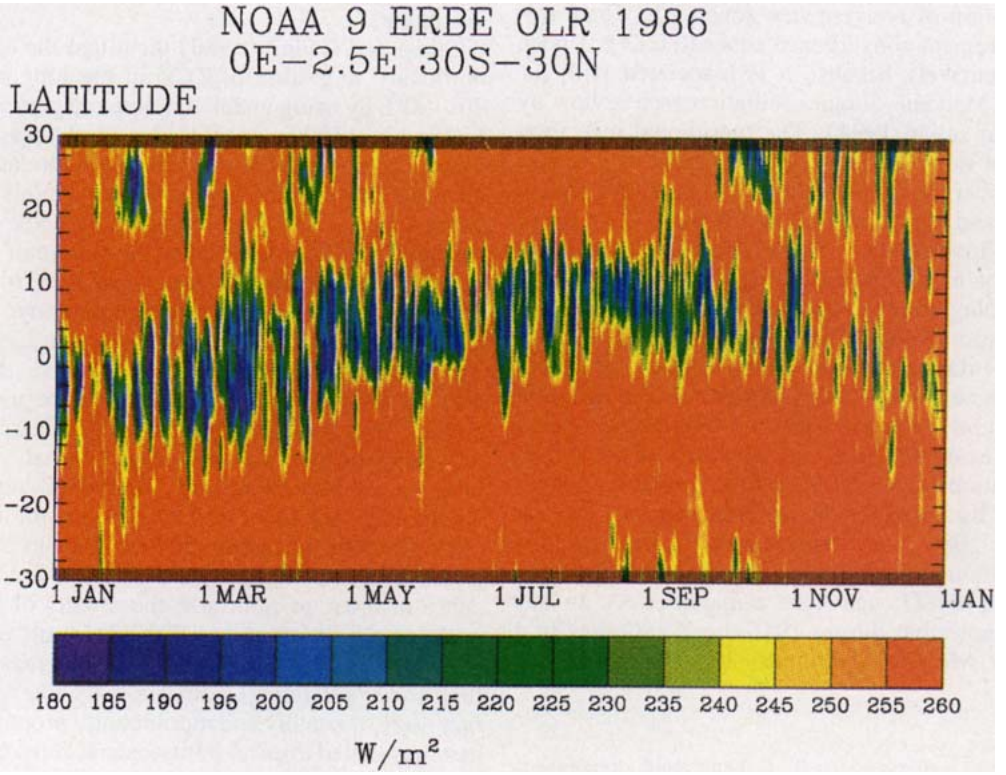

FIG. 2. Latitude–time variation of daily OLR in West Africa (0°–2.5°E) in 1986.

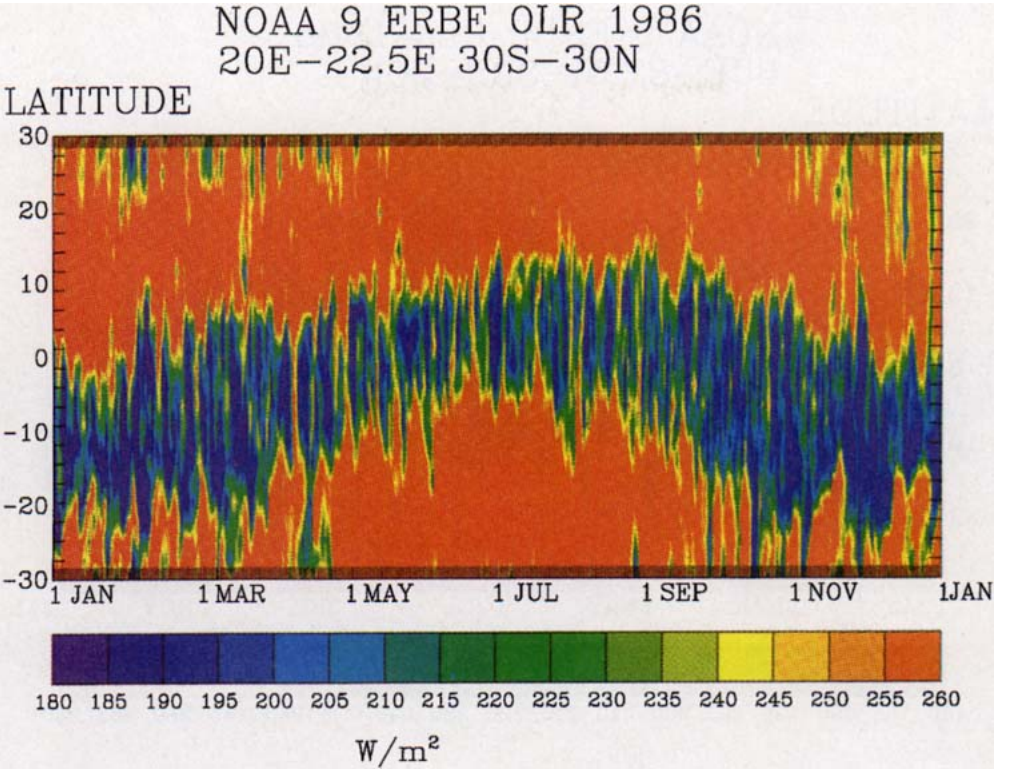

FIG. 3. Latitude–time variation of daily OLR in central Africa (20°–22.5°E) in 1986.

spatial or temporal filtering. We use the 2.5° × 2.5° daily OLR data from ERBE in the present study. The zonal migration of TCZ is around 5°–10° per day, and hence the zonally migrating TCZ will move out of a 2.5° longitude domain rapidly. Hence, a latitude–time plot of OLR at a single longitude (2.5° wide) reveals primarily those TCZ that migrate in the meridional direction.

Section 2 examines the nature of meridional migration in different regions of the Tropics using the daily ERBE OLR data. Section 3 discusses the various mechanisms that can cause the meridional migration of convergence zones. Section 4 discusses the wind–evaporation feedback mechanism and its importance in the Atlantic and east Pacific Oceans. Section 5 summarizes the results. An appendix lists symbols that are used in the analysis.

2. Meridional migration in various regions

We examine the nature of seasonal and intraseasonal meridional migration of TCZ in different regions of the Tropics. TCZ are identified as spatially and temporally coherent regions with daily OLR below 200 W m^{-2}. The pattern of seasonal and intraseasonal variation of TCZ in the Tropics strongly depends upon the relative disposition of the continents and oceans. We classify the different regions of the Tropics as 1) equatorial continent (African continent, 20°–40°E and South America, 40°–80°W), 2) equatorial ocean and subtropical continent (Indian and west Pacific Oceans), and 3) oceanic (east Pacific and Atlantic Oceans). These regions may be considered to be different experiments in the response of the atmosphere to land–ocean interactions. We examine the latitudinal movement of the TCZ at the longitudes indicated in the map of Fig. 1.

In West Africa and the eastern Atlantic Ocean (0°–2.5°E) the seasonal migration of TCZ (Fig. 2) is between 10°S and 10°N. On an intraseasonal scale both northward and southward propagations occur. In this region the TCZ does not move onto the African continent. In central Africa (20°–22.5°E) the seasonal migration (Fig. 3) is from 20°S to 10°N with the TCZ being more active in the Southern Hemisphere. The TCZ does not move beyond 10°N during the boreal summer. This is a special feature of the African continent and it will be shown later that it is related to the meridional variation of net radiation at the top of the atmosphere.

At the latitude of the Indian subcontinent (80°–82.5°E) the seasonal migration of TCZ (Fig. 4) occurs

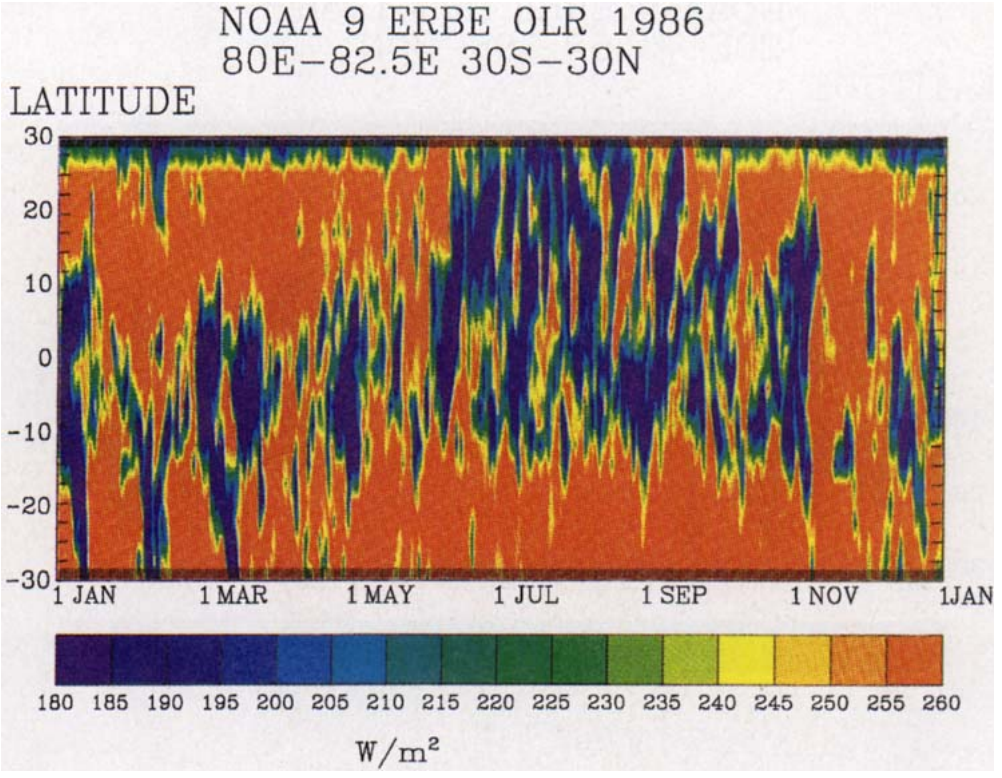

FIG. 4. Latitude–time variation of daily OLR in Indian subcontinent (80°–82.5°E) in 1986.

between 5°S and 20°N. On an intraseasonal scale there is southward migration from the equator during boreal winter and northward migration during boreal summer. All the meridionally propagating TCZ seem to originate in the equatorial region (10°S–10°N). The period between the meridionally propagating events is approximately one month and hence one may be tempted to conclude that the meridionally propagating TCZ must be linked to the eastward propagating TCZ along the equator. Wang and Rui (1990) showed, however, the meridional propagation of TCZ during the period June–August is usually not linked to the eastward migrating TCZ along the equator. In July 1986, however, the eastward migrating equatorial TCZ reached the longitude 80°E on 6 July 1986, after which a TCZ propagated northward and moved onto the Indian subcontinent. During the other months of the summer there is no evidence of eastward migrating TCZ along the equator, and hence the northward-propagating modes occurring in June, August, and September must be classified as "independent" northward-propagating modes following the classification of Wang and Rui (1990).

In the Philippines (120°–122.5°E), there is a seasonal migration (Fig. 5) from 10°S to 10°N, while on the intraseasonal scale northward migrations dominate. In the west Pacific Ocean (150°–152.5°E) the seasonal migration is limited, while on the intraseasonal scale the northward migrating events dominate even during the austral summer (Fig. 6). At the date line (180°–182.5°E), the seasonal migration of TCZ is from 15°S to 5°N, and on the intraseasonal scale the northward-migrating modes dominate (Fig. 7). Across the regions 150°E–180° there are migrations toward the equator from 30°S. In the east Pacific Ocean (117.5°–120°W), there is no seasonal migration of TCZ, while on the intraseasonal scale northward migrations dominate (Fig. 8). Although northward migrations dominate across regions from 150°E to 120°W, in the regions 60° to 120°E the intraseasonal TCZ migrated from the equatorial region to the north or south depending on season. This difference could be due to the effects of land–sea contrast that are important in the region 60°–120°E but nonexistent in the region east of 150°E–120°W.

In the Amazon basin (67.5°–70°W) the TCZ migrates seasonally from 15°S to the equator (Fig. 9). The intraseasonal migration is primarily northward. In the Atlantic Ocean (27.5°–30°W) the seasonal migration of TCZ is between 5°S and 5°N, while on an intraseasonal scale northward migration can be seen during the period October to December (Fig. 10).

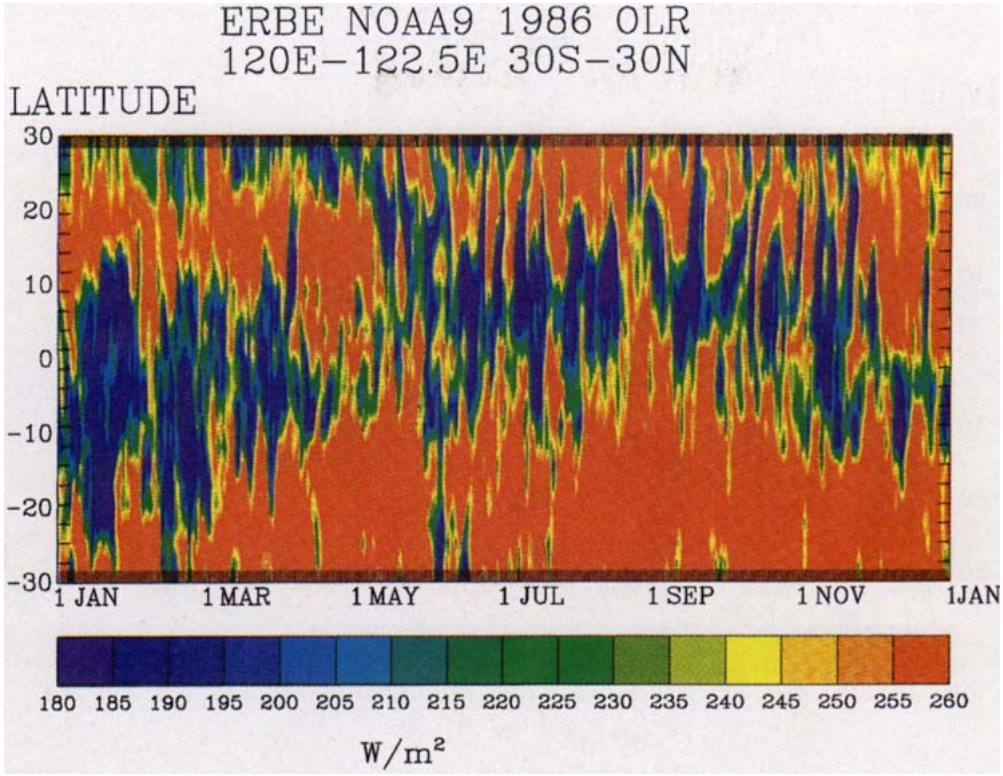

FIG. 5. Latitude–time variation of daily OLR in Philippines (120°–122.5°E) in 1986.

3. Mechanisms for meridional migration

Figures 2–10 show a wide variety of TCZ behavior from one region of the Tropics to another. Northward (during boreal summer) and southward (austral summer) propagating TCZ occur primarily in the longitudes of Asia and Australia (60°–150°E). In these regions the TCZ originate in the equatorial region and move northward or southward depending upon the season. In all other regions the predominant direction of movement of TCZ is northward. For a symmetric earth the direction of propagation would vary with season. The pattern of meridional migration in the Asia–Australia regions (60°–150°E) is very different from that in the African continent or in South America. The Asia–Australia regions are unique because of the warm equatorial ocean straddled by a large continent to the north or south.

We argue that the warm equatorial ocean provides the moisture source and a region for the genesis of TCZ, while the strong north–south land–sea contrast leads to the meridional migration of TCZ. This argument is consistent with the results of Webster and Lau (1977), who have shown that meridional migration of TCZ is observed in a simple symmetric model if and only if there is a continent located north or south of the equator. The TCZ that forms (or arrives by zonal migration) at a specific longitude along the equator in these regions will tend to move into the hemisphere where the solar heating of the continent is dominant. Gadgil and Srinivasan (1990) and Srinivasan et al. (1993) used the simple symmetric climate model of Webster (1983) to show that the dominant factor governing the meridional migration of TCZ in that model (when there is land–sea contrast) is the meridional gradient in the moist static stability.

The absence of substantial meridional migration in the African continent can be explained on the basis of the theoretical results of Neelin and Held (1987) and of Charney (1975). Neelin and Held (1987) showed that for a sustained weather pattern (lasting several days) in the continental regions, the net energy convergence in the troposphere can be assumed to be equal to the net radiation at the top of the atmosphere (also called the planetary net radiation). For a sustained pattern, the energy storage term in the atmosphere and the ground can be neglected, and the net positive radiation flux must be balanced by the release of latent heat that is brought into the region by convergence of the lower-level flow. On the other hand, Charney demonstrated that negative planetary net radiation can be maintained over a long period only by subsidence of the atmosphere, in which potential energy is radiated as the air

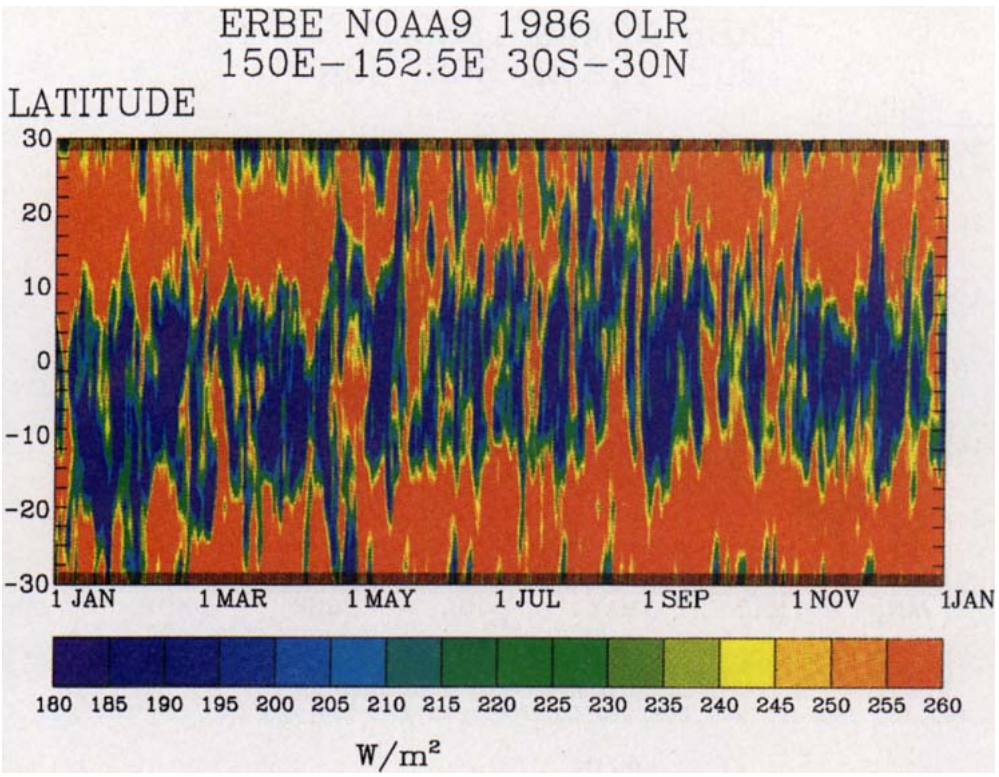

FIG. 6. Latitude–time variation of daily OLR in west Pacific Ocean (150°–152.5°E) in 1986.

subsides. This is the mechanism of the atmospheric flow over a desert (Charney 1975; Charney et al. 1977). Thus, TCZ can be sustained in a continental region if and only if the planetary net radiation is positive. In the African continent, the planetary net radiation is positive in the boreal summer in the region around 5°N as shown in Fig. 11. Hence, we do not observe any meridional migration of TCZ in the African continent during the boreal summer. This result indicates the strong influence of the seasonal mean conditions on the intraseasonal variation of TCZ. The meridional migration of TCZ (in the seasonal or intraseasonal scale) is limited in Africa because of the presence of regions with negative planetary net radiation in the subtropics. The periodicity of meridional migration in these regions is explained by ground hydrology feedbacks as discussed by Webster (1983).

Because there is no land–sea contrast in this region, the northward migration during the boreal winter in the east Pacific and Atlantic Oceans requires a different explanation. Moreover, one would not expect northward migration from the equator during the boreal winter because the solar heating maximum will be in the Southern Hemisphere. The meridional gradient in SST in these regions is not sufficiently large as to cause a meridional gradient in moist static stability that is large enough to cause migration of the TCZ. A large part of the gradient of moist static stability between land and ocean is due to the decrease of relative humidity over the land relative to that over the ocean. Hence we cannot invoke the mechanism suggested by Gadgil and Srinivasan (1990) and Srinivasan et al. (1993). Recently, Emanuel (1993) has shown that wind–evaporation feedback can cause poleward migration of disturbances when there are mean easterlies in the lower troposphere. The zonal winds in the lower troposphere in the tropical Atlantic and tropical Pacific Oceans are mainly easterly. Hence, the presence of northward migration in boreal winter in the Atlantic and east Pacific Oceans could be due to the wind–evaporation feedback mechanism proposed by Emanuel (1993). This mechanism cannot be invoked for the region 60°–150°E because of the presence of continents wherein the wind-evaporation feedback is much more complex than over oceans. In the continental regions the fluctuations in evaporation are linked to ground hydrology feedbacks, while in oceanic regions the fluctuations in the evaporation are primarily due to the fluctuations in the zonal wind. We discuss in section 4 the role of wind–evaporation feedback in the poleward migration of disturbances when there are mean easterly winds in the Tropics.

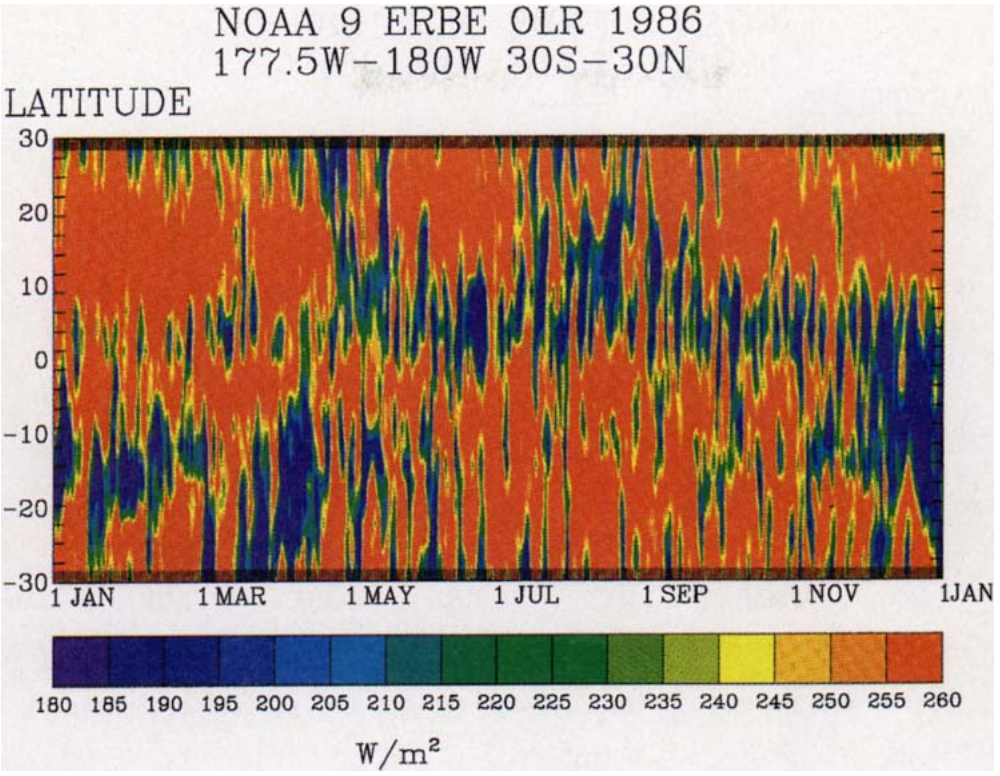

FIG. 7. Latitude–time variation of daily OLR at the date line (180°–182.5°E) in 1986.

4. Wind–evaporation feedback mechanism

Wind–evaporation feedback, first postulated by Emanuel (1987) and Neelin et al. (1987), provides an explanation of meridional migration of TCZ. They used two different approaches but arrived at essentially the same conclusion regarding the role of wind-induced surface heat exchange (WISHE) on Kelvin waves. There is an enormous amount of energy in the tropical oceans that can be transferred to the atmosphere to drive circulations. The easterlies ahead of an eastward-propagating trough are increased, resulting in increased transfer of enthalpy from the ocean, which warms the troposphere when it is distributed by convection. Emanuel (1993) demonstrated that the introduction of a time lag between convergence and precipitation eliminated the tendency for the waves with the largest wavenumber (and frequency) to amplify most. He showed that westward-propagating mixed Rossby–gravity waves with a zonal wavenumber in the range 3–6 had the highest growth rates if the time lag was around one to two hours. He also found that the waves in the midlatitude beta plane showed a tendency for poleward migration. He did not discuss the possibility of poleward migrations in the equatorial beta-plane solutions. We treat the equatorial beta plane case in greater detail here.

We begin with the basic equations in the equatorial beta plane as given by Emanuel (1993):

$$U_t + \bar{U}U_x - yV + \Phi_x = 0, \quad (1)$$

$$V_t + \bar{U}V_x + yU + \Phi_y = 0, \quad (2)$$

$$\Phi_t + \bar{U}\Phi_x + (U_x + V_y) = B\{U_x + V_y\} + A\{U\}. \quad (3)$$

In the above equations, the independent and dependent variables are nondimensionalized by the length scale $(C/\beta)^{1/2}$ and the timescale $(C\beta)^{-1/2}$, where β is the gradient of the Coriolis parameter and C is the gravity wave speed for a dry atmosphere, which we take to be 50 m s^{-1}. The terms in curly brackets in the right-hand side of the energy equation are evaluated with a time lag of τ. This time lag between convergence (or evaporation) and precipitation was introduced by Davies (1979) and used by Emanuel (1993) to account for the time it takes for the clouds to form and precipitation to occur. The nondimensional wind–evaporation feedback parameter A is defined such that it is positive when the mean zonal wind is easterly and negative when the mean zonal wind is westerly. The nondimensional latent heating parameter B has been termed the precipitation efficiency by Emanuel (1993), who argued that

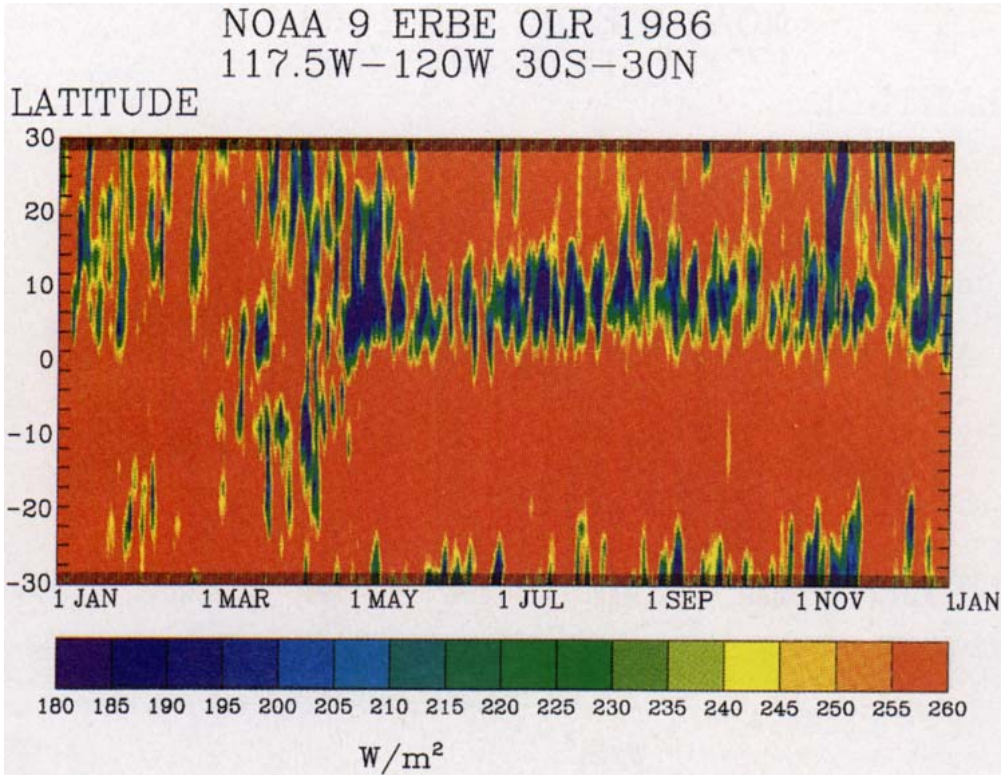

FIG. 8. Latitude–time variation of daily OLR in the east Pacific (117.5°–120°W) in 1986.

this parameter equals zero if the temperature lapse rate is dry adiabatic and equals one if the temperature lapse rate is moist adiabatic. Dissipation terms are neglected for simplicity, as the existence of the waves of interest do not depend on the effects of friction and Rayleigh cooling.

We assume that the dependent variables vary periodically in time and longitude as $\exp[i(K_X x - \omega t - K_X \bar{U} t)]$, where K_X is the nondimensional zonal wavenumber and ω is the nondimensional Doppler-shifted frequency. We then obtain a single equation for the perturbation nondimensional meridional velocity as

$$V_{yy} - yDV_y + \left(G - \frac{y^2}{\chi}\right)V = 0, \tag{4}$$

where

$$D = \frac{iAe^{i\omega\tau}}{\chi\omega}, \tag{5}$$

$$\chi = 1 - Be^{i\omega\tau}, \tag{6}$$

$$G = \frac{\omega^2}{\chi} - K_X^2 - \frac{K_X}{\omega} - iAe^{i\omega\tau}\frac{(K_X + \omega^{-1})}{\chi}. \tag{7}$$

Equation (4) is transformed to the canonical form by the transformation

$$V = \tilde{V}\exp\left(D\frac{y^2}{4}\right) \tag{8}$$

to

$$\tilde{V}_{yy} + (F - E^2y^2)\tilde{V} = 0, \tag{9}$$

where

$$F = \frac{\omega^2}{\chi} - K_X^2 - \frac{K_X}{\omega} - iAe^{i\omega\tau}\left(\frac{K_X + 0.5\omega^{-1}}{\chi}\right), \tag{10}$$

$$E^2 = \frac{1}{\chi} + \frac{D^2}{4}. \tag{11}$$

The dispersion relation for obtaining eigenvalues is

$$F = (2n + 1)E. \tag{13}$$

The solution for the meridional velocity is now written in terms of the Hermite polynomials H_n as

$$V(y) = H_n(yE^{1/2})\exp(\delta y^2), \tag{14}$$

where $\delta = D/4 - E/2$. Because of the time delay associated with the wind–evaporation feedback and the latent heating, δ is complex. For the $n = 0$ case, which is the mixed Rossby–gravity wave, Eq. (14) can be written

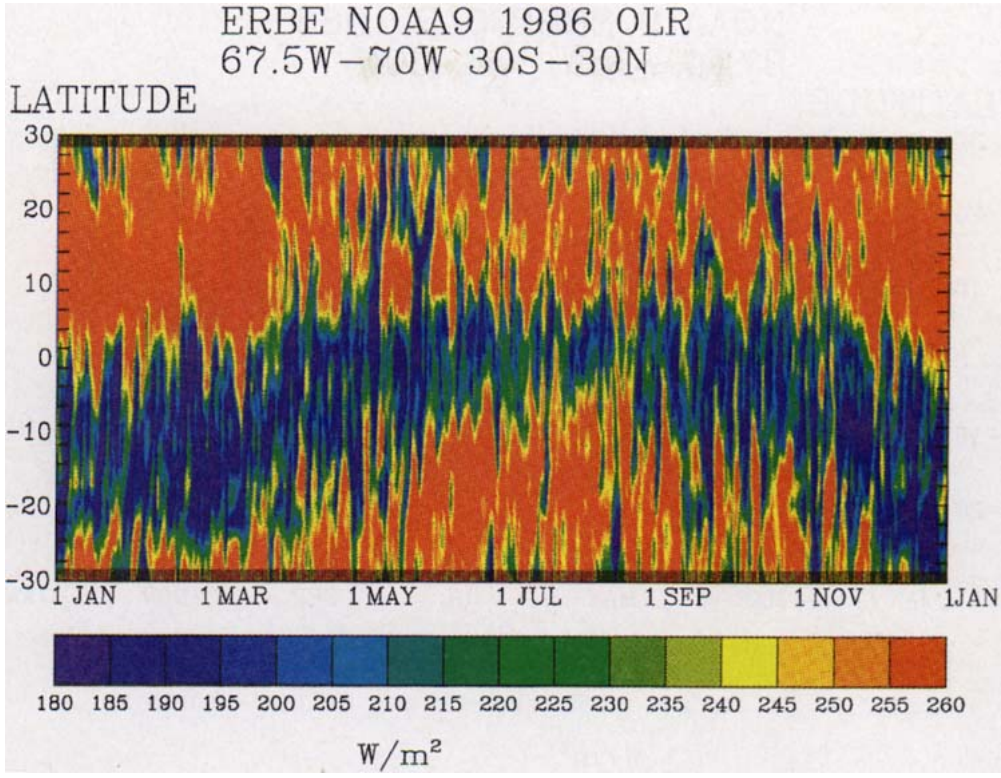

FIG. 9. Latitude–time variation of daily OLR in the Amazon basin (67.5°–70°W) in 1986.

$$V(y) = \exp(\delta_R y^2) \exp(\delta_I y^2).$$

This form demonstrates that the $V(y)$ solution has a magnitude that is Gaussian in y and a phase which varies as $\delta_I y^2$. When the x and t variations are included, the total phase of the wave is $\phi = \delta_I y^2 + K_X \chi - \omega t - K_X U t$. The constant phase lines in the latitude–time domain or the latitude–longitude domain are thus parabolae. If δ_I and K_X have different signs, the waves emanate from the equator; otherwise, they converge toward the equator. The WKB solution developed by Emanuel (1993) approximates the waves by replacing the parabolic wave front by a local tangent.

We focus our attention on the mixed Rossby–gravity wave ($n = 0$) because Liebmann and Hendon (1990) have identified the existence of mixed Rossby–gravity (MRG) wave in the equatorial regions of the Atlantic and the Pacific Oceans. The C_D is assumed to be 0.001 and Δq around 0.008 g kg^{-1} so that the wind-evaporation parameter A is around -0.25. The latent heating parameter is assumed to be around 0.9 and the nondimensional time lag τ around 0.2. This corresponds to dimensional time lag of 1.7 h. Emanuel (1993) argues that observations suggest that the suitable time lag is 20 min to several hours and deals with time lags of 1 and 2 h. Figure 12 shows the variation of growth rate with wavenumber for two different values of the latent heating parameter B. When $B = 0.9$, the growth rates are much larger than when $B = 0.6$. This indicates that westward-migrating waves are amplified by the wind–evaporation feedback and the maximum growth rate occurs for zonal wavenumbers in the range of 5–10. Furthermore, MRG waves will amplify in mean easterly winds if and only if there is sufficient moisture in the lower troposphere (or precipitation efficiency is high in the terminology of Emanuel 1993).

The variation of growth rate with nondimensional Doppler-shifted frequency is shown in Fig. 13. The growth rate attains a peak when the nondimensional Doppler-shifted frequency is around 0.4 (for $B = 0.9$). This corresponds to a period of 4 days when there is an easterly wind of 5 m s^{-1}. Note that the growth rate peaks more sharply in the frequency domain than in the wavenumber domain. This is because the frequency does not vary much with wavenumber (Fig. 14). Liebmann and Hendon (1990) have shown that MRG waves in wavenumber range 5–10 and with the time period of 4–6 days are prominent in the observed meridional and zonal winds in the equatorial Atlantic and Pacific Oceans during the months September–December. A MRG wave with wind–evaporation feedback and latent heating is able to simulate most of the observed features of the TCZ movements in the equatorial

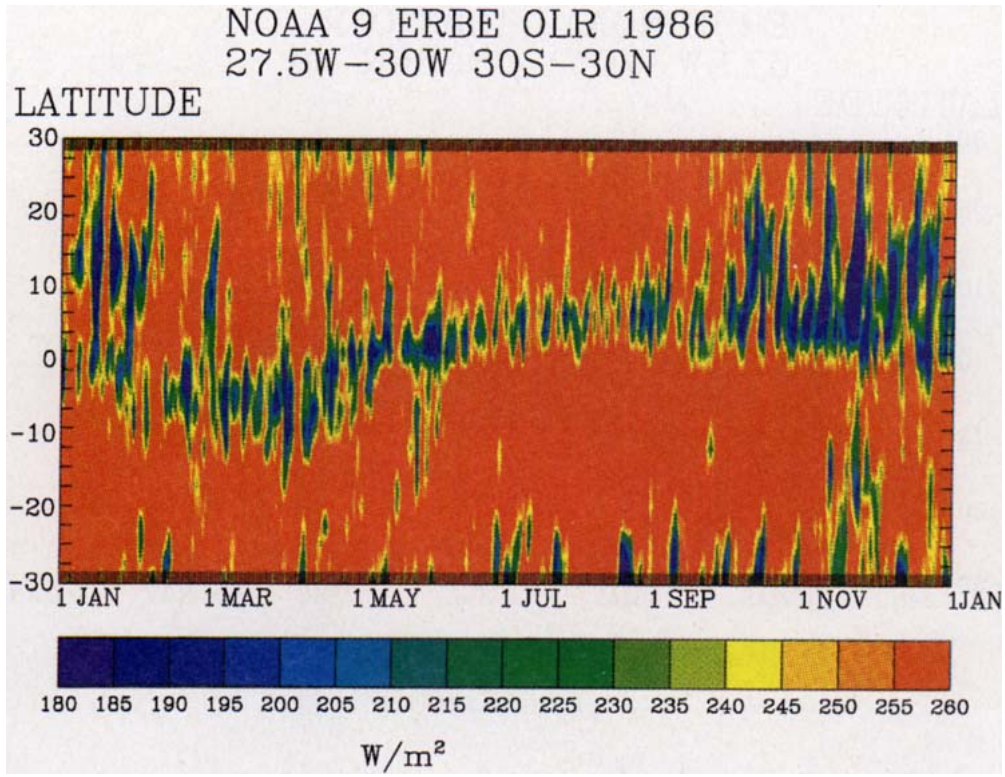

FIG. 10. Latitude–time variation of daily OLR in the Atlantic Ocean (27.5°–30°W) in 1986.

Atlantic and Pacific Oceans. Northward-migrating TCZ are prominent in the OLR data in the Atlantic and Pacific Oceans during the period October–December. These northward-migrating TCZ have a time period around 5–6 days and move poleward at the rate of 3°–5° per day. The MRG waves have zero divergence at the equator.

The temporal and meridional dependence of divergence induced by MRG wave is given by the following expression for divergence:

$$U_X + V_y = \mathrm{Re}\left\{\frac{[iK_X + (i\omega + AK_X e^{i\omega\tau}/\omega)2\delta]y}{(i\omega - iK_X^2\chi/\omega + AK_X e^{i\omega\tau}/\omega)} \times \exp[i(K_X X - \omega t) + \delta y^2]\right\}.$$

Figure 15 shows the variation of divergence with latitude and time for a MRG wave with a wavelength of 8000 km. The parabolic latitude–time phase relation of the wave discussed earlier appears as meridional migration of divergence and convergence zones. The rate of meridional migration is around 4° per day, which is comparable to the rate of meridional migration of TCZ in the Atlantic and east Pacific Oceans. Figure 16 shows the variation of daily OLR in the Atlantic Ocean (27.5°–30°W) during October 1986. The rate of meridional migration of low OLR regions is comparable to the rate of meridional migration of convergence zones in the MRG wave (Fig. 15). The northward migration of low OLR regions (or convergence zones) is more prominent than the northward migration of high OLR regions (or divergence zones). This could be because convergence causes a large reduction in OLR while divergence causes a smaller increase in OLR.

The MRG wave coupled with the wind–evaporation feedback mechanism produces poleward migrating convergence zones whose wavelength, period, and rate of meridional migration are similar to the observations of Liebmann and Hendon (1990) and the OLR data presented in this paper. The MRG waves show southward migration of convergence zones in the Southern Hemisphere, which is not discernible in the observations. The wind–evaporation feedback mechanism causes the amplification of westward-migrating MRG waves if and only if the nondimensional latent-heating parameter B is sufficiently close to 1.0. The value of latent-heating parameter is thus dependent on whether a given region is subject to convergence or divergence (in the monthly mean sense).

For a longitudinal wavelength of 8000 km, there are solutions for waves with periods greater than 2 days

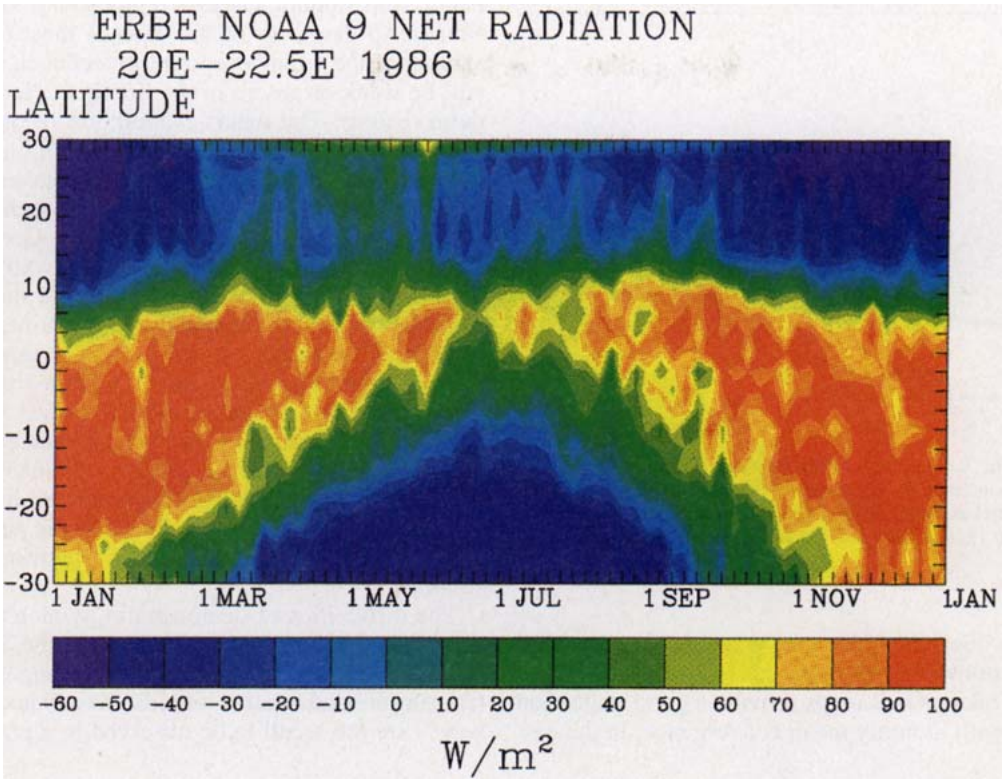

FIG. 11. Latitude–time variation of net radiation at the top of the atmosphere in central Africa (20°–22.5°E) during 1986.

for doubling times greater than 6 h for A values between -0.2 and -0.3, for all other parameters held constant. When the longitudinal wavelength is doubled, to 16 000 km, such solutions exist for A values between -0.1 and -1. For a longitudinal wavelength of 4000 km, there are no solutions for such waves for any A between -1 and 1. Thus, at the equator the WISHE

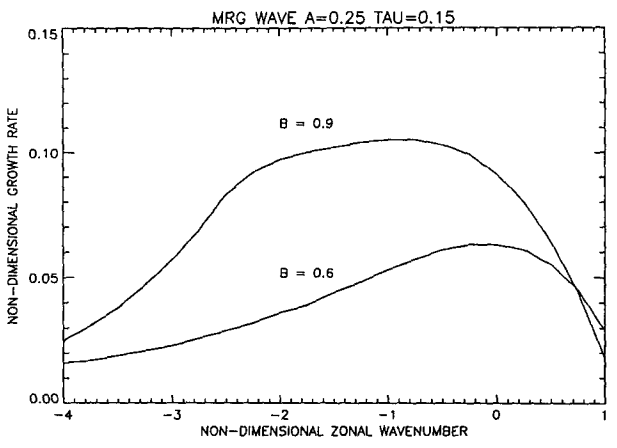

FIG. 12. The variation of nondimensional growth rate with nondimensional wave number for mixed Rossby–gravity wave with wind–evaporation parameter $A = 0.25$, nondimensional time lag $\tau = 0.15$, and two values of latent-heating parameter B (0.6, 0.9).

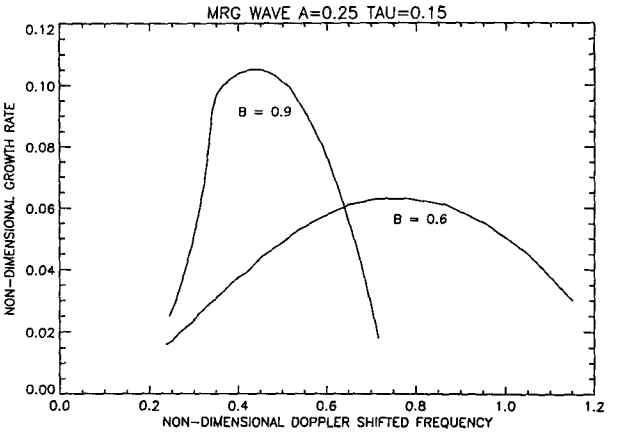

FIG. 13. The variation of nondimensional growth rate with nondimensional Doppler-shifted frequency for mixed Rossby–gravity wave with wind–evaporation parameter $A = 0.25$, nondimensional time lag $\tau = 0.15$, and two values of latent-heating parameter B (0.6, 0.9).

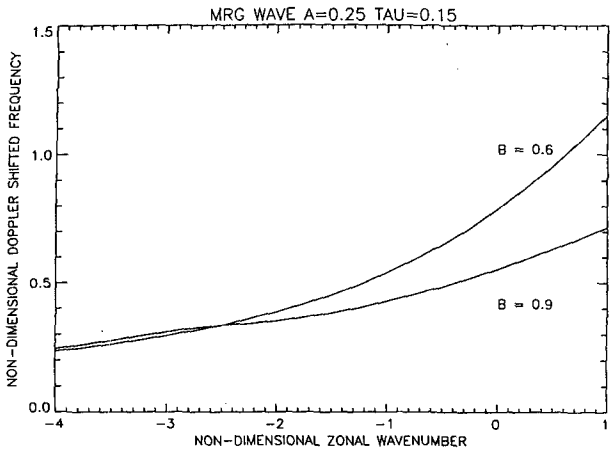

FIG. 14. The variation of nondimensional Doppler-shifted frequency with nondimensional wavenumber for mixed Rossby–gravity wave with wind-evaporation parameter $A = 0.25$, nondimensional time lag $\tau = 0.15$, and two values of latent heating parameter B (0.6, 0.9).

mechanism does not operate for waves as short as 4000 km but favors waves of longer east–west extent.

Monthly mean OLR maps provide a good indication of regions with monthly mean convergence. In the east Pacific and Atlantic Oceans, regions with low OLR are situated to the north of the equator most of the year, and hence the wind–evaporation feedback mechanism will be weak or absent in the Southern Hemisphere in these regions. The wind–evaporation feedback mechanism will cause an equatorward migration of TCZ in the equatorial regions subject to mean westerlies. In the boreal summer, mean westerlies are seen along the equator in the Indian and west Pacific Oceans. There is, however, little evidence of equatorward migration of TCZ in these regions during the boreal summer. This could be because of the presence of continents in these regions. The nature of wind–evaporation feedback over continents is very different from that over the oceans, and hence one would not expect the models developed by Emanuel (1987) and Neelin et al. (1987) for oceanic regions to be valid in continental regions. Webster (1983) has shown that complex hydrological feedbacks in the continents can cause the poleward migration of TCZ in the Asian continent during the boreal summer.

The difficulties of demonstrating which mechanism is responsible for observed waves in the Tropics are discussed by Emanuel (1993). The changes on virtual temperature and relative humidity associated with these waves are too small to be observed in a practical field

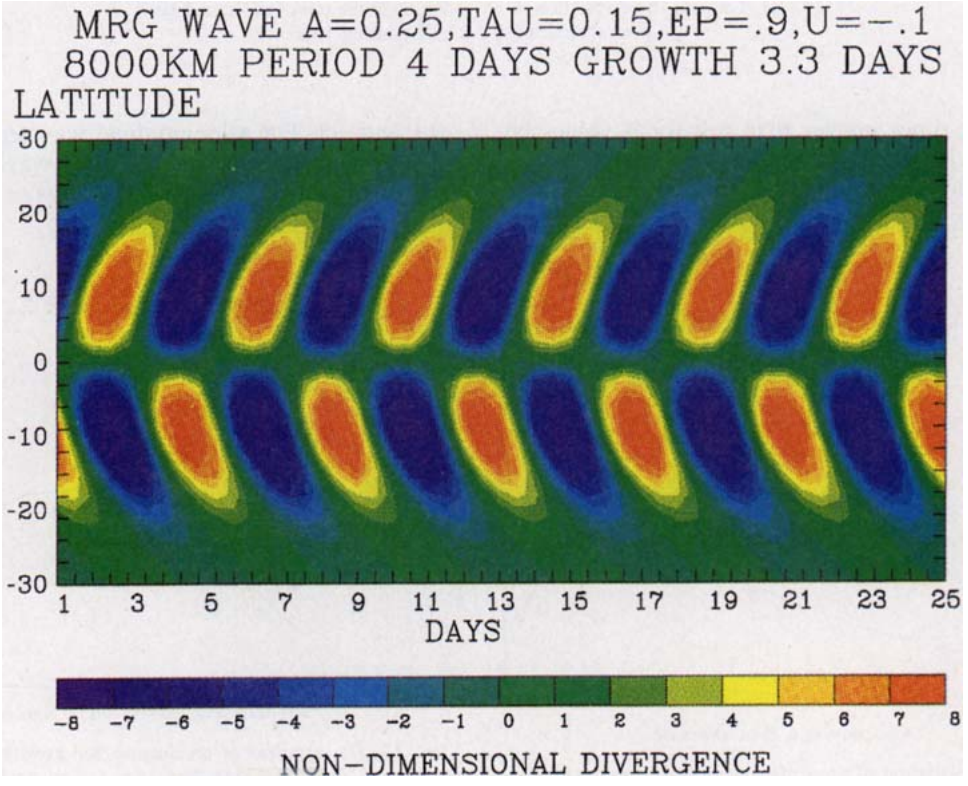

FIG. 15. Latitude–time variation of divergence induced by mixed Rossby–gravity wave with wavelength of 8000 km and period of 4 days.

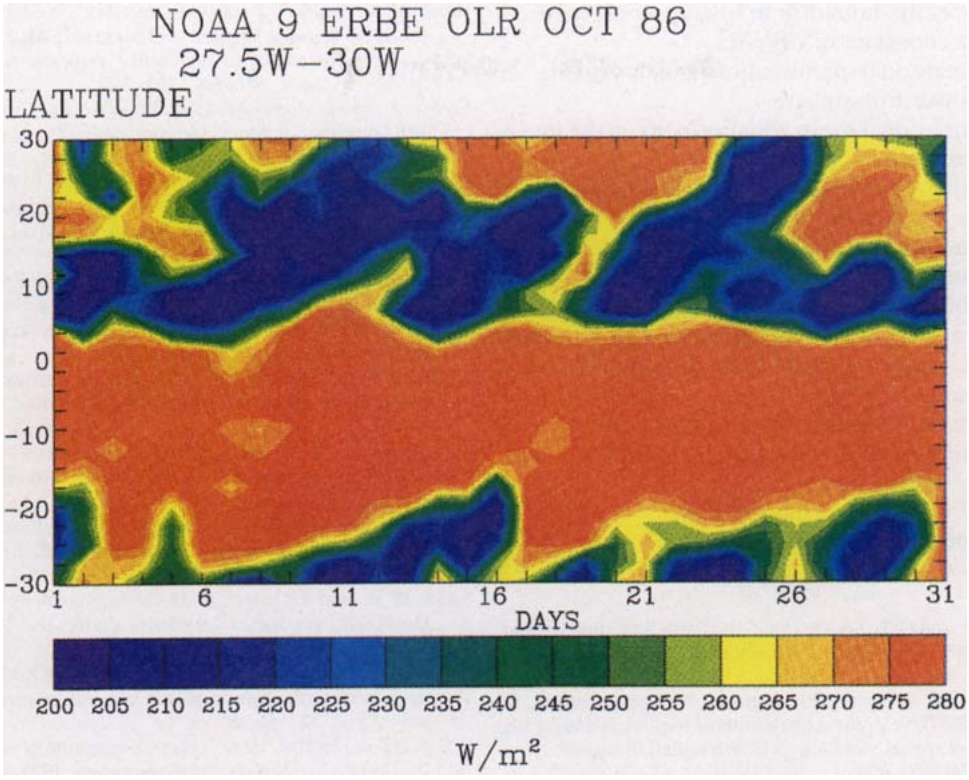

FIG. 16. Latitude–time variation of daily OLR in the Atlantic Ocean (27.5°–30°W) in October 1986.

experiment. Emanuel (1987) suggested tests that could be done with a general circulation model that could resolve the importance of various potential mechanisms in the numerical solutions. However, this approach would not apply for comparison of theory to observations. Webster (1983) pointed out that model "results must be considered as suggestive."

5. Conclusions

Daily OLR data reveal a variety of patterns of meridional migration in differing regions of the Tropics, showing that different mechanisms are important in different regions of the Tropics. In the West Africa–east Atlantic Ocean region, the TCZ moves with the seasons but moves little on intraseasonal timescales. The intraseasonal poleward migrations of the TCZ in the Indian and west Pacific Oceans can be attributed to the strong land–sea contrast in these regions, as demonstrated by Webster (1983) using a simple model. The existence of northward migrations of TCZ in the east Pacific and Atlantic Oceans can be explained by the wind–evaporation feedback mechanism proposed by Emanuel (1993). It is shown that the convergence induced by mixed–Rossby gravity waves with wind–evaporation feedback migrates poleward in the presence of mean easterlies. When the time lag between convection and precipitation is around a few hours, the MRG waves with period around 4 days attain the maximum growth rate and can thus explain the fluctuations with this time period in the wind data in the Atlantic and east Pacific Oceans. The divergence of the waves has parabolic trajectories in the latitude–time domain.

Acknowledgments. This work was undertaken when one of the authors (JS) was a NASA-NRC resident research associate at NASA Langley Research Center on leave from Indian Institute of Science, Bangalore, India.

APPENDIX

Symbols

A	$LR\rho g\Delta qC_D/2\Delta pC_pC(C\beta)^{1/2}$, nondimensional wind–evaporation parameter
B	$L\bar{q}R/2C_pC^2$, nondimensional latent heating parameter
C	Gravity wave speed in the dry atmosphere
C_D	Drag coefficient in the bulk aerodynamic formula
C_p	Specific heat of dry air
g	Acceleration due to gravity
L	Latent heat of vaporization

$\bar{q}$ Mean specific humidity in lower troposphere
R Ideal gas constant of dry air
U Nondimensional perturbation zonal velocity in the lower troposphere
$\bar{U}$ Nondimensional mean zonal velocity in the lower troposphere
V Nondimensional perturbation meridional velocity in the lower troposphere
x Nondimensional zonal coordinate
y Nondimensional meridional coordinate
β Meridional gradient of the Coriolis parameter
Δq Difference between saturation specific humidity at the surface and the specific humidity at the anemometer level
Δp Pressure depth of the lower troposphere
Φ Nondimensional perturbation geopotential in the lower troposphere
ρ Density of dry air at the surface
τ Nondimensional time

REFERENCES

Barkstrom, B. R., and G. L. Smith, 1986: The Earth Radiation Budget Experiment: Science and implementation. *Rev. Geophys.*, **24,** 379–390.

Brooks, D. R., E. F. Harrison, P. Minnis, J. T. Suttles, and R. S. Kandel, 1986: Development of algorithms for understanding the temporal and spatial variability of earth radiation balance. *Rev. Geophys.*, **24,** 422–438.

Charney, J. G., 1975: Dynamics of deserts and drought in the Sahel. *Quart. J. Roy. Meteor. Soc.*, **101,** 193–202.

——, W. J. Quirk, S.-H. Chow, and J. Kornfield, 1977: A comparative study of the effects of albedo change on drought in semi-arid regions. *J. Atmos. Sci.*, **34,** 1366–1385.

Davies, H. C., 1979: Phase-lagged wave-CISK. *Quart. J. Roy. Meteor. Soc.*, **105,** 325–353.

Emanuel, K. A., 1987: An air–sea interaction model of intraseasonal oscillations in the Tropics. *J. Atmos. Sci.*, **44,** 2324–2340.

——, 1993: The effect of convective response time on WISHE modes. *J. Atmos. Sci.*, **50,** 1763–1775.

Gadgil, S., and J. Srinivasan, 1990: Low frequency variations of tropical convergence zones. *Meteor. Atmos. Phys.*, **44,** 119–132.

Liebmann, B., and H. H. Hendon, 1990: Synoptic-scale disturbance near the equator. *J. Atmos. Sci.*, **47,** 1463–1479.

Madden, R. A., and P. R. Julian, 1994: Observations of the 40–50-day tropical oscillation—A review. *Mon. Wea. Rev.*, **122,** 814–837.

Minnis, P., and E. F. Harrison, 1984: Diurnal variability of regional cloud and clear-sky radiative parameters derived from GOES data. Part II: November 1978 cloud distributions. *J. Climate Appl. Meteor.*, **23,** 1012–1031.

Neelin, J. D., and I. M. Held, 1987: Modeling tropical convergence based on the moist static energy budget. *Mon. Wea. Rev.*, **115,** 3–12.

——, ——, and K. H. Cook, 1987: Evaporation–wind feedback and low-frequency variability in the tropical atmosphere. *J. Atmos. Sci.*, **44,** 2341–2348.

Seager, R., and S. E. Zebiak, 1994: Convective interaction with dynamics in a linear primitive equation model. *J. Atmos. Sci.*, **51,** 1307–1331.

Sikka, D. R., and S. Gadgil, 1980: On the maximum cloud zone and the ITCZ over Indian longitudes during the Southwest Monsoon. *Mon. Wea. Rev.*, **108,** 1840–1853.

Srinivasan, J., S. Gadgil, and P. J. Webster, 1993: Meridional propagation of large-scale monsoon convective zones. *Meteor. Atmos. Phys.*, **52,** 15–35.

Wang, B., and H. Rui, 1990: Synoptic climatology of transient tropical intraseasonal convection anomalies: 1975–85. *Meteor. Atmos. Phys.*, **44,** 43–61.

Webster, P. J., 1983: Mechanism of monsoon low-frequency variability: Surface hydrology effects. *J. Atmos. Sci.*, **40,** 2110–2127.

——, and K. M. W. Lau, 1977: A simple ocean–atmosphere climate model: Basic model and a simple experiment. *J. Atmos. Sci.*, **34,** 1063–1084.